frontiers | Frontiers in Ecology and Evolution

TYPE Review
PUBLISHED 26 September 2023
DOI 10.3389/fevo.2023.1226349

OPEN ACCESS

EDITED BY
Mingyu Zhao,
Chinese Academy of Sciences (CAS), China

REVIEWED BY
Shijun Jiang,
Hohai University, China
Mingtao Li,
Linyi University, China
Wei Shi,
Chengdu University of Technology, China

*CORRESPONDENCE
Yinggang Zhang
ygzhang@nigpas.ac.cn
Benjamin J. W. Mills
B.Mills@leeds.ac.uk
Tianchen He
tianchenhe@hhu.edu.cn

RECEIVED 21 May 2023
ACCEPTED 12 September 2023
PUBLISHED 26 September 2023

CITATION
Zhang Y, Mills BJW, He T, Hu X and Zhu M (2023) Modeling hyperthermal events in the Mesozoic-Paleogene periods: a review. *Front. Ecol. Evol.* 11:1226349. doi: 10.3389/fevo.2023.1226349

Modeling hyperthermal events in the Mesozoic-Paleogene periods: a review

Yinggang Zhang[1]*, Benjamin J. W. Mills[2]*, Tianchen He[2,3]*, Xiumian Hu[4] and Maoyan Zhu[1]

[1]State Key Laboratory of Palaeobiology and Stratigraphy, Nanjing Institute of Geology and Palaeontology, Chinese Academy of Sciences, Nanjing, China, [2]School of Earth Environment, University of Leeds, Leeds, United Kingdom, [3]College of Oceanography, Hohai University, Nanjing, China, [4]State Key Laboratory of Mineral Deposit Research, School of Earth Sciences and Engineering, Nanjing University, Nanjing, China

Hyperthermal events, which are characterized by rapid and extreme warming, occurred at several points throughout the Mesozoic to Paleogene periods. Model simulation studies have been conducted to investigate the mechanisms behind these events, including the carbon fluxes required to drive observed warming and isotope dynamics, the impact of warming on continental weathering, seawater pH, ocean anoxia, and the mechanism that terminated the warming. Studies using simple box models, Earth system box models, or 3D Earth system models have suggested that warming had a significant biogeochemical impact and would enhance continental weathering, increase ocean anoxia, and drive marine acidification. However, the magnitudes of these impacts remain debated and require further modeling work, as do the reconstructions of carbon fluxes and compositions. This review provides an overview of the current state of knowledge on hyperthermal events and proposes possible modeling development directions to better understand the causes and impacts of these events. Particularly, new long-term 'semi-spatial' Earth system models are promising tools for providing new solutions and perspectives on the biogeochemical responses to warming events and the carbon fluxes behind hyperthermal events from the Mesozoic to Paleogene periods.

KEYWORDS

hyperthermal events, Mesozoic-Paleogene, Earth system box model, biogeochemistry, carbon cycle

Introduction

Hyperthermal events, characterized by rapid and extreme global warming, have significant impacts on the Earth's surface environment and biosphere through multiple factors such as ocean acidification, anoxia, acid rain, and aridity, ultimately resulting in mass extinctions (Montoya-Pino et al., 2010; Clarkson et al., 2015; Penn et al., 2018; Shen et al., 2019; Rush et al., 2021). At the present day, we are living through a >1°C global

warming event caused by anthropogenic carbon emissions (IPCC, 2022). However, the mechanisms and environmental effects of past global warming remain unclear, hindering our understanding of the mechanisms of global warming and its bio-environmental effects. Climate warming extremes have occurred numerous times, particularly during the Mesozoic to Paleogene eras, which saw the Permian-Triassic Boundary event (PTB, ~252 Ma), early Toarcian Oceanic Anoxic Event (TOAE, ~183 Ma), early Aptian oceanic anoxic event (OAE 1a, ~120 Ma), Cenomanian-Turonian oceanic anoxic event (OAE 2, ~94Ma), and the Paleocene-Eocene Thermal Maximum (PETM, ~56 Ma) (see Figure 1) (Hu et al., 2020).

These past hyperthermal events offer valuable geological windows for studying the mechanisms of global warming and its bio-environmental effects. For instance, the PTB event at the end of the Permian (~252 Ma) was characterized by a rapid increase in atmospheric carbon dioxide (CO_2), leading to global warming of 6–11°C (Penn et al., 2018; Shen et al., 2019), ocean acidification (Payne et al., 2010; Clarkson et al., 2015; Silva-Tamayo et al., 2018), and marine anoxia (Song et al., 2012). The PTB event resulted in the extinction of 81% of marine species (Stanley, 2016) and 70% of terrestrial species (Sahney and Benton, 2008). The carbon emission responsible for the PTB hyperthermal event has been linked to the Siberian Traps Large Igneous Province (LIP) based on their strong temporal association (Joachimski et al., 2020). Similarly, other hyperthermal events (TOAE, OAE 1a, OAE 2, and PETM) are also believed to be causally linked to LIPs that share a temporal association with them. These associated LIPs are Karoo-Ferrar Province (Percival et al., 2016), Ontong-Java Plateau (Bauer et al., 2017), Caribbean-Madagascar flood basalts (Turgeon and Creaser, 2008), and North Atlantic Igneous Province (Gutjahr et al., 2017), respectively (see Figure 1).

Numerical modeling has proven to be an effective approach for quantitatively investigating the driving mechanisms for hyperthermal events, including the identification of potential carbon sources, the amount of carbon that drove warming (e.g., Cui et al., 2021b; Wu et al., 2023), and the resulting environmental impacts. These models span a range of complexity and spatial resolutions: from simple box models and Earth system box models to 3D Earth system models. Simple box models represent the major geochemical or geophysical processes in the geological cycles of the elements or isotopes of interest, by treating each reservoir as a box and calculating the fluxes among these reservoirs. 'Earth system box models', which incorporate the interactions among the primary chemical cycles in the atmosphere, ocean, land, and biosphere, represent these processes with a higher level of complexity than simple box models for single chemical species.

One of the most widely used Earth system box models is the Carbon-Oxygen-Phosphorus-Sulfur-Evolution model (COPSE) (Bergman et al., 2004; Lenton et al., 2018) which involves the surficial C, O, P, and S cycles among the atmosphere, ocean, land, sediments, and biosphere. For example, Ullmann et al. (2020) used the COPSE model to predict seawater C isotopes, temperature, weathering, nutrient dynamics, and ocean anoxia intensity to compare with geological evidence for the TOAE event, suggesting that the C cycle perturbation of the TOAE was caused by the injection of carbon derived from the interaction of LIPs with sedimentary organic matter and methane.

In contrast to the simple/Earth system box models, 3D Earth system models integrate the interactions of the atmosphere, ocean, land, ice, and biosphere across a spatially-defined grid, focusing on the expressions of physiochemical processes and energy exchange, allowing estimation of local physiochemical processes and states of each grid. Like the box models, 3D models use a defined number of boxes or containers to store information about concentrations of species of interest, but in these models, the boxes are assigned specific spatial locations, thus they are not usually termed to be 'box models'. An example of a low-resolution 3D Earth system model (intermediate complexity) is the Carbon centric-Grid Enabled Integrated Earth system model (cGENIE; Ridgwell et al., 2007), while an example of a high-resolution 3D Earth System

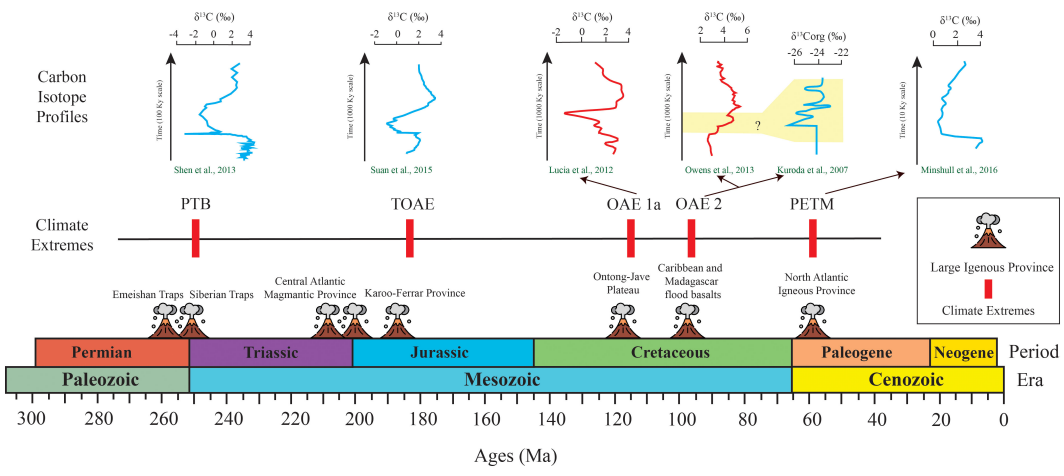

FIGURE 1
Hyperthermal events, their possible related large volcanism activities, and their typical seawater carbon isotope pattern from the Mesozoic to Paleogene. Note: the seawater carbon isotope patterns are from Kuroda et al. (2007), Di Lucia et al. (2012), Owens et al. (2013), Shen et al. (2013), Suan et al. (2015), and Minshull et al. (2016).

Model is the Community Earth System Model (CESM, available at https://www.cesm.ucar.edu). Even the low-resolution 3D models have substantially longer computation times than the simple box models or Earth system box models, meaning they typically produce 'snapshots' of climate and biogeochemistry for a certain time in the past or geologically short (<100 kyr) transient simulations.

This review explores recent modeling studies of hyperthermal events and their implications for warming mechanisms and bio-environmental influences. As hyperthermal events typically last more than 100 kyr, we will particularly focus on simple box models and Earth system box models, which can be applied for these timescales, and will discuss how these models are being extended to include 3D representations of steady-state climate (Goddéris et al., 2014; Mills et al., 2021), bringing their functionality closer in line with the 3D Earth system models.

Previous modeling work on climate extremes

In this section, we briefly introduce each hyperthermal event and summarize the modeling work on these events chronologically: PTB, TOAE, OAE 1a, OAE 2, and PETM.

The PTB event

As previously mentioned, the PTB event led to the extinction of most life on Earth, both on land and in the ocean, due to a combination of factors such as ocean acidification, anoxia, and acid rain (Clarkson et al., 2015; Penn et al., 2018; Dal Corso et al., 2022; Wang et al., 2023). Although the interplay of kill mechanisms during this event is still debated, it is widely agreed to have been ultimately triggered by massive amounts of greenhouse gases such as CO_2 released into the atmosphere during the emplacement of the Siberian Traps LIP (Figure 2). This process led to a global temperature increase of approximately 6–11°C within a few thousand years, as evidenced by oxygen isotope records (Penn et al., 2018; Shen et al., 2019). The PTB event is characterized by a negative seawater C isotope excursion of 3–8‰ (Shen et al., 2013; Joachimski et al., 2020) (see Figure 1 and Table 1).

Using calculated annual air temperature and runoff from a one-dimensional energy balance model, Grard et al. (2005) applied a box model of biogeochemical carbon and alkalinity cycles to investigate the negative $\delta^{13}C$ excursion (NCE) driver. By applying time-dependent forcing functions for the eruptive phase and mass extinctions, the model generated a seawater NCE of approximately −3‰. The authors suggested that volcanic eruptions with ~19,200 Pg mantle carbon with a −5‰ $\delta^{13}C$ value (Table 1) could generate the negative C isotope anomaly, while a reduction in primary productivity that decreased the removal of ^{13}C-depleted organic carbon from the ocean also contributed. However, when combined with proxy data for atmospheric CO_2, the carbon source was determined to have significant contributions of ^{13}C-depleted carbon (<−5‰) (Table 1) (Payne et al., 2010; Wu et al., 2021).

Observations of negative calcium (Ca) isotope excursion during the PTB, when combined with a box model that coupled the C and Ca cycles, suggested that the average $\delta^{13}C$ of CO_2 released was more likely near −15‰ (Payne et al., 2010). This conclusion was further

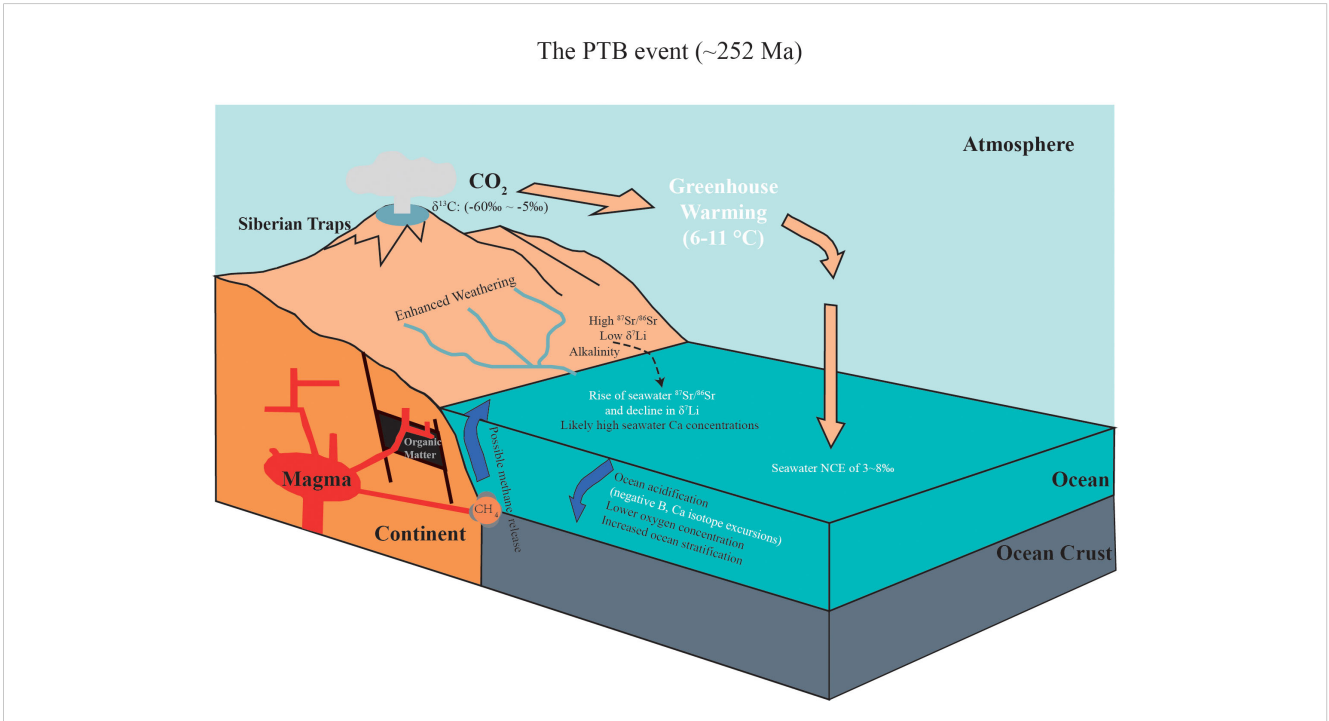

FIGURE 2
Driving mechanisms and environmental impacts of the PTB hyperthermal event (modified from Hu et al., 2020).

10.3389/fevo.2023.1226349

TABLE 1 Comparison of hyperthermal events showing the global warming magnitude, carbon isotope excursion, duration, and proposed possible carbon sources.

Hyperthermal events	Total duration (and onset duration)	Global temperature	C isotope excursion type	C isotope excursion magnitude	Total amount of C emissions	Possible C resources	Model type	Reference
PTB	~660 kyr (~58 kyr)	6–11°C	NCE	3–8‰	~19,200 Pg	Mantle ^{13}C-depleted CO_2; $\delta^{13}C$: −5‰	Simple box model of the C cycle	Grard et al. (2005)
					13,200–21,600 Pg	Mixed carbon sources but necessary with mantle-derived CO_2; $\delta^{13}C$: −11‰ to −28‰	Simple box model that coupled the C and Ca cycles	Payne et al. (2010)
					~36,000 Pg	Largely volcanic CO_2 source; ~−15‰	Earth system model of intermediate complexity (cGENIE)	Cui et al. (2021b)
					3,900–12,000 Pg	Organic matter and methane release scenarios; $\delta^{13}C$: −25‰ to −60‰	Simple carbon isotope mass balance	Wu et al. (2021)
					~5,000 Pg	A combination of remobilized organic matter and mantle-derived carbon; $\delta^{13}C$: −15‰ to −25‰	Simple box model (LOSCAR)	Shen et al. (2022)
					~26,000 Pg	Two-phased C release: 1. ~5,000 Pg thermogenic C of −60 to −20‰, 2; ~21,000 Pg volcanic C of −20 to 0‰	Earth system model of intermediate complexity (cGENIE)	Wu et al. (2023)
					18,000–30,000 Pg	A predominantly volcanic CO_2 source; $\delta^{13}C$: −8 to −12‰	Simple box model (LOSCAR)	Wang et al. (2023)
TOAE	300–900 kyr (~150 kyr)	5–10°C	NCE	3–8‰	1,500–2,700 Pg	Methane-hydrate dissociation; $\delta^{13}C$: −60‰	Simple carbon isotope mass balance	Hesselbo et al. (2000)
					2,600–4,400 Pg	Magma-intruded organic-rich rock	Simple mass balance calculations	McElwain et al. (2005)
					/	A thermogenic CO_2 source; $\delta^{13}C$: −6 to −14‰	Simple box model of the Ca cycle	Brazier et al. (2015)
					/	A mixed source of mantle CO_2 with organic C (~−7‰) and methene (~−60‰)	Earth system box model (COPSE)	Ullmann et al. (2020)
OAE 1a	~2.1 Myr (~395 kyr)	2–6°C	An NCE at its onset followed by a broad PCE	NCE (~4‰) PCE (2–5‰)	~20,000–100,000 Pg C	Mantle C emissions; $\delta^{13}C$: −6‰	Simple box model (LOSCAR)	Bauer et al. (2017)
					~2,000–450,000 Pg	Thermo- and/or biogenic methane resouce (−70 to −30‰) to a dominantly volcanic source (−20 to 0‰)	Earth system model of intermediate complexity (cGENIE)	Adloff et al. (2020)

(Continued)

TABLE 1 Continued

Hyperthermal events	Total duration (and onset duration)	Global temperature	C isotope excursion type	C isotope excursion magnitude	Total amount of C emissions	Possible C resources	Model type	Reference
OAE 2	200–>900 kyr (~50 kyr)	2–10°C	An NCE at its onset followed by a broad PCE	NCE (~3‰) PCE (2–5‰)	/	Volcanic LIP degassing; $\delta^{13}C$: −5‰	Simple box models (the Cretaceous Ocean Box Model with 27 ocean boxes, COBM) and an Earth system box model (GENESIS)	Flögel et al. (2011)
					19,000–33,000 Pg C	Volcanic LIP degassing; $\delta^{13}C$: −5‰	A simple box model of the atmosphere-ocean C cycle	Kuroda et al. (2007)
PETM	150–220 kyr (8–23 kyr)	5–8°C	NCE	2–7‰	>1,100–2,100 Pg	Thermal dissociation of oceanic hydrate; $\delta^{13}C$: −60‰	Carbon mass balance calculation	Dickens et al. (1995)
					/	Rapid burning of accumulated terrestrial organic carbon	Simple box models of the C and S cycles	Kurtz et al. (2003)
					~6,800 Pg	A combination of methane, volcanic CO_2, organic matter-derived CO_2; $\delta^{13}C$: −22‰	Earth system model of intermediate complexity (cGENIE)	Panchuk et al. (2008)
					1,500–3,000 Pg	Thermal dissociation of oceanic hydrate; $\delta^{13}C$: −50‰	Simple box model (LOSCAR)	Zeebe et al. (2009) Frieling et al. (2016)
					900–1,400 Pg	Combined CH_4 and CO_2 resouce; $\delta^{13}C$: −60 to −50‰	Simple box model of the C cycle	Carozza et al. (2011)
					2,500–12,500 Pg	Possibly a mixed C souce of mantle-derived CO_2, biogenic methane and thermogenic CO_2. 1. CH_4: 2,500 Pg C, $\delta^{13}C$: −60 to −50‰; 2. Organic matter-derived CO_2: 12,500 Pg C, $\delta^{13}C$: ~−22‰	Earth system model of intermediate complexity (cGENIE)	Cui et al. (2011)
					10,200–12,200 Pg	A predominantly volcanic CO_2 source; $\delta^{13}C$: −17 to −11‰	Earth system model of intermediate complexity (cGENIE)	Gutjahr et al. (2017)
					~7,500 Pg	Organic matter-derived CO_2; $\delta^{13}C$: ~−22‰	A simple box model of the C cycle	Cui et al. (2021a)

The global warming magnitude, carbon isotope excursion, and duration refer to Hu et al., 2020 and references therein.

supported by simulations with the Long-term Ocean-atmosphere Sediment CArbon cycle Reservoir Model (LOSCAR; a type of box model, Zeebe, 2012), where a combination of mantle sources (~−5‰) and organic matter-derived CO_2 (~−30‰) (Shen et al., 2022) or volcanic CO_2 sources ranging from −8 to −12‰ (Wang et al., 2023) was required to match the observed NCE pattern (Table 1). Similarly, a massive (~36,000 Pg C) and rapid emission of C source (~−15‰) (Cui et al., 2021b) or two-phased C release (1. ~5,000 Pg thermogenic C of −60 to −20‰, 2. ~21,000 Pg volcanic C of −20 to 0‰) (Wu et al., 2023) was required to drive the observed NCE pattern (Table 1) in the cGENIE Earth system model with intermediate complexity (Ridgwell et al., 2007).

In addition to thermogenic or volcanic CO_2 release, the collapse of vegetation on land has also been suggested to impact the NCE

pattern significantly. This is particularly true for explaining the sudden negative shift superimposed on the relatively gentle negative excursion (Figure 1). Such a shift has been explained through the use of box modeling of coupled C, P, and mercury (Hg) cycles (Dal Corso et al., 2020) and the strontium (Sr) cycle (Song et al., 2015).

Combinations of other geochemical proxies with numerical modeling techniques for elemental cycles have led to further hypotheses for environmental change during the PTB event. By utilizing a simple Sr ocean box model to simulate the accelerated rise of seawater $^{87}Sr/^{86}Sr$ during the PTB event, it was proposed that the continental weathering rate in the Early Triassic was enhanced by more than 1.9 times compared to the late Permian (Table 2), due to the intensification of runoff and vegetation die-off (Song et al., 2015). Similarly, a simple lithium (Li) ocean box model and light seawater Li isotopic signatures during the P–T transition were interpreted as evidence for enhanced continental weathering (Sun et al., 2018).

In contrast to the consensus on the increased continental weathering, primary productivity during the P–T transition is debated. High nutrient levels and therefore high primary productivity was suggested using the cGENIE model to explain the gradient of C isotopes versus water depth (Meyer et al., 2011), while the nitrogen isotope record indicated lower nutrient levels and low productivity caused by suppressed upwelling (Grasby et al., 2016). Due to uncertain changes in primary productivity, its variations during the P–T transition were not included in Figure 2.

Ocean acidification is believed to have played a major role in the P–T mass extinction, as evidenced by seawater boron (B) and Ca isotopes and models of those systems (Payne et al., 2010; Clarkson et al., 2015; Silva-Tamayo et al., 2018). The observed negative isotopic excursions of C and Ca, along with a forward box model of the C and Ca cycles, suggested a CO_2-driven ocean acidification scenario (Figure 2) accompanied by intensified weathering of Ca-bearing rocks during the PTB event (Payne et al., 2010; Silva-Tamayo et al., 2018). With further constraints on seawater pH variations from B isotopes, a box model of the C cycle was utilized to simulate seawater C and B isotope fluctuations during the PTB, suggesting that the acidifying effects of CO_2 released during the formation of the Siberian Traps were buffered for approximately 150 kyr until global ocean acidification occurred (Clarkson et al., 2015). In addition to ocean acidification, global warming could also lead to increased ocean stratification (Figure 2) and decreased ocean circulation due to lower oxygen solubility and increased runoff into high-latitude oceans, as demonstrated by the CESM (Penn et al., 2018). These factors could help account for the extinction of marine species during the PTB event (Penn et al., 2018).

There has been relatively little modeling work on the demise of the PTB event. Existing work suggests the termination of the warming was related to the weakening of volcanism (Dal Corso et al., 2020), enhanced continental weathering (Song et al., 2015; Sun et al., 2018), and processes such as organic carbon burial and carbonate formation (Silva-Tamayo et al., 2018) which played important roles in reducing atmospheric CO_2 levels back to pre-event levels.

TOAE

TOAE, also called the 'Jenkyns event', occurred during the Early Jurassic period (~183 Ma) and was characterized by the deposition of organic-rich sediments on a global scale (Suan et al., 2013). The event is widely attributed to a sudden increase in atmospheric CO_2 levels, which is thought to have led to a greenhouse warming effect of over 5°C (Figure 3 and Table 1) (McElwain et al., 2005; Suan et al., 2015). Isotope analysis reveals that the TOAE is associated with an NCE in both marine and terrestrial environments, with a magnitude of −3‰ to −8‰ (Suan et al., 2015; Them et al., 2017a) (Figure 1). This event has been linked to the early magmatism of the Karoo-Ferrar LIP (Figure 1) (Percival et al., 2016).

The perturbation in the carbon cycle was initially attributed to the sudden release of light C from either magma-intruded organic-rich rocks (Kump and Arthur, 1999) or marine gas hydrates (Hesselbo et al., 2000). McElwain et al. (2005) estimated the marine gas hydrates reservoir and conducted a simple carbon cycle calculation, using CO_2 proxy data and the NCE pattern to support the carbon source from magma-intruded organic-rich rock (~2,600–4,400 Pg C) (Figure 3 and Table 1). Subsequently, negative Ca isotope excursions found during the TOAE, together with an ocean box model of the Ca cycle, were used to constrain the continental weathering input to the ocean and the causes of the NCE (Brazier et al., 2015). This study suggested that injections of carbon with a range of −6‰ to −14‰ were the most likely cause for the NCE, supporting the carbon source of thermogenic CO_2 (McElwain et al., 2005). However, recent COPSE modeling of the NCE and temperature variations during TOAE suggests that the interactions of the Karoo-Ferrar large igneous province with organic C (~−7‰) and methene (~−60‰) both contributed to the global warming and the NCE (Ullmann et al., 2020) (Table 1).

Regarding the impact of the TOAE warming event, Brazier et al. (2015) utilized an ocean box model of the Ca cycle to study the causes of the negative $\delta^{44}/^{40}Ca$ excursions during the TOAE, and proposed that a transient 90% decrease of carbonate accumulation due to ocean acidification followed by a 5-fold increase in continental weathering rates (Table 2) were required to match the Ca isotope record. However, this estimated enhance factor for weathering was later adjusted to 2.15–5.30 times (Table 2) compared to the pre-event baseline by Them et al. (2017b) based on a positive osmium (Os) isotope excursion and box modeling of the Os cycle. Finally, the COPSE model was used to match the NCE and temperature variations, and it was found that the enhanced factor of continental weathering required was approximately 1.67 times (Table 2) (Ullmann et al., 2020).

Continental weathering also played a vital role in ending the TOAE by enhancing CO_2 sequestration as a negative feedback mechanism (Them et al., 2017b). Moreover, the increased fluxes from continental weathering would have brought more nutrients into the ocean, increasing organic carbon burial (Ullmann et al., 2020). This, in turn, likely contributed to the termination of the TOAE. The increased organic carbon burial was suggested to be caused by stratification and anoxia resulting from a sluggish ocean

TABLE 2 Comparison of hyperthermal events showing modeling weathering enhancement factors and related proxy records.

Hyperthermal events	Proxy	Enhance weathering factor	Reference
PTB	Sr (Rise of seawater $^{87}Sr/^{86}Sr$)	1.9 times	Song et al. (2015)
	Li (Light Li isotopic values during PTB)	18 times	Sun et al. (2018)
TOAE	Ca (Negative $\delta^{44}/^{40}Ca$ excursion)	5 times	Brazier et al. (2015)
	Os (Positive $^{187}Os/^{188}Os$ excursion)	2.15–5.3 times	Them et al. (2017b)
	C isotope and temperature variations	~1.67 times	Ullmann et al. (2020)
OAE 1a	Ca, Sr (Slightly decline in $^{87}Sr/^{86}Sr$, negative $\delta^{44}/^{40}Ca$ excursion)	3 times	Blättler et al. (2011)
	Li, Sr, Os, Ca (Negative $^{187}Os/^{188}Os$ and $\delta^{7}Li$ excursions)	2.5 times	Lechler et al. (2015)
	S (Falling of $\delta^{34}S$seawater)	3 times	Bauer et al. (2022)
OAE 2	Ca, Sr (Short-lived increase in $^{87}Sr/^{86}Sr$, negative $\delta^{44}/^{40}Ca$ excursion)	3 times	Blättler et al. (2011)
	Li, Sr, Os, Ca (Negative $^{187}Os/^{188}Os$, $\delta^{44}/^{40}Ca$, $\delta^{7}Li$, and $^{87}Sr/^{86}Sr$ excursions)	1–3 times	Pogge Von Strandmann et al. (2013)
	Sr (A rise of seawater $^{87}Sr/^{86}Sr$ following a broad decline)	1.8 times	Nana Yobo et al. (2021)
PETM	Li (Negative $\delta^{7}Li$ excursion both in seawater and local weathering inputs)	~1.5 times	Pogge Von Strandmann et al. (2021)

circulation (Figure 3), which was simulated in general circulation models such as the Fast Ocean-Atmosphere Model (FOAM) (Dera and Donnadieu, 2012; Baroni et al., 2018) and Princeton Ocean Model (POM) (Bjerrum et al., 2001).

The sulfur (S) cycle during the TOAE also drew the attention of geologists, especially in reconstructing seawater sulfate concentrations. Forward box modeling of the S cycle was used to simulate the extended recovery of seawater sulfate S isotopes after the TOAE. This suggested a Toarcian marine sulfate concentration of 4–8 mM (Gill et al., 2011). This low sulfate concentration was further supported by additional seawater sulfate S isotope data and the maximum sulfate concentrations (Han et al., 2022) calculated using the 'rate method', which infers the sulfate concentration based on the rate of change of sulfur isotopes (Algeo et al., 2015).

OAE 1a

OAE 1a, which occurred in the early Aptian (~120 Ma) during the mid-Cretaceous, was a period of rapid and extreme global warming (Figure 4), which has been estimated to be between 2 and 6°C (Ando et al., 2008). This event was also associated with widespread anoxia in the oceans and high atmospheric CO_2 concentrations (Jenkyns, 2010; Percival et al., 2021), and had significant impacts on both marine and terrestrial ecosystems, causing changes in nutrient cycles, shifts in primary productivity, and biological turnover (e.g., Keller et al., 2011). The event is marked by widespread preservation of organic matter in marine settings (Jenkyns, 2010) and a significant NCE at its onset, followed by a broad positive carbon isotope excursion (PCE) with a magnitude of 2–5‰ (Figure 1) (Di Lucia et al., 2012). This event has been causally linked to the eruption of the Ontong Java Plateau LIP (Figure 1) (Tejada et al., 2009; Keller et al., 2011; Kashiwagi, 2016; Bauer et al., 2017).

Based on large un-radiogenic Os isotope shifts during OAE 1a, box modeling of the Os isotope excursions suggests a rapid 6–10 times increase in volcanic activity during the event (Bauer et al., 2017) and/or weathering of a huge amount (~30–60%) of the Ontong Jave Plateau (Tejada et al., 2009). Additionally, the LOSCAR C-cycle box model (Zeebe, 2012) was used to investigate the impact of increased volcanic emissions on the carbon cycle, suggesting that a ~4 times rise in mantle carbon emissions ($\delta^{13}C$: ~−6‰) (Table 1) could explain the abrupt negative carbon isotope excursion (NCE) during the OAE 1a alone (Bauer et al., 2017).

Subsequently, the cGENIE model was employed to assimilate an atmospheric CO_2 reconstruction and the carbon isotope record of OAE 1a, suggesting a shift from a ^{13}C-depleted reservoir (e.g., thermo- and/or biogenic methane from sill intrusions: −70 to −30‰) towards a dominantly volcanic source (e.g., LIPs: −20 to 0‰) (Table 1) (Adloff et al., 2020). Recently, hydrothermal activity has been proposed as the primary cause of the un-radiogenic Os isotope shift based on additional Os isotope data (Matsumoto et al., 2022), which may support the hypothesis of a shifting carbon source (Adloff et al., 2020).

To explain the negative Ca and Sr isotope shifts, an oceanic box model with coupled Sr and Ca isotope cycles was used to show that a threefold increase in continental weathering (Table 2) and a 20% increase in hydrothermal activity for 5 Myr could drive these changes (Blättler et al., 2011). The relative contributions of hydrothermal activity and continental weathering were later revised to a 1.7-fold increase in hydrothermal activity with a 2.5-

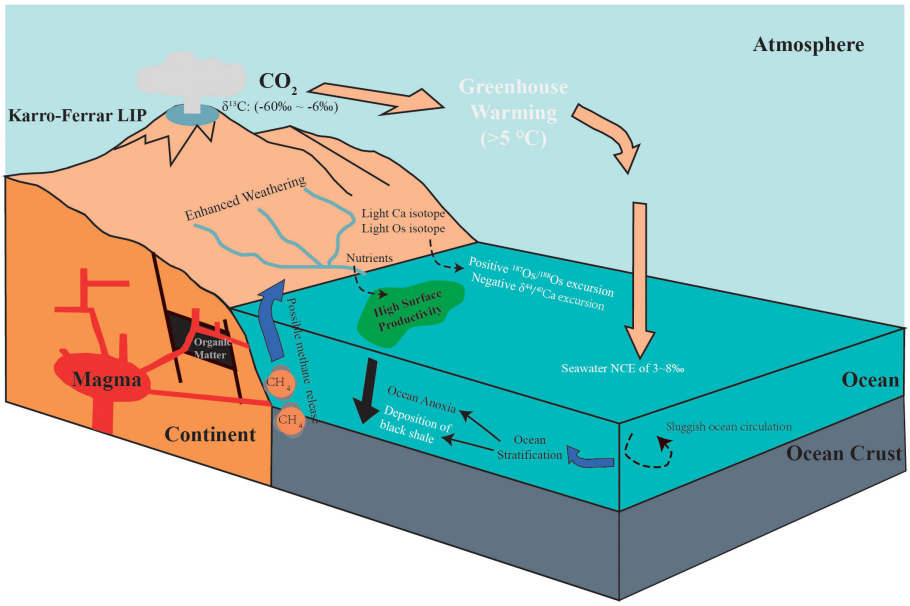

FIGURE 3
Driving mechanisms and environmental impacts of TOAE (modified from Hu et al., 2020).

fold enhancement in continental weathering (Table 2) for 6 Myr to match the Li, Sr, Os, and Ca isotope variations during OAE 1a in an ocean box model of coupled elemental cycles (Lechler et al., 2015). To match the S isotope record under low seawater sulfate concentrations, a 4.2-fold increase in hydrothermal inputs and a threefold increase in weathering fluxes (Table 2) over 500 kyr, combined with increased evaporite and pyrite burial, was necessary within an ocean box model of the S cycle (Bauer et al., 2022). An S-cycle box model previously showed that increased weathering inputs would increase marine sulfate concentration from a low background value, which was responsible for decreased seawater $\delta^{34}S$ isotopes (Gomes et al., 2016).

As for the termination of OAE 1a, a carbon cycle model based on the GEOCARB model (Berner and Kothavala, 2001) was applied to study the atmospheric CO_2 variations (Kashiwagi, 2016). The study suggested that the end of the OAE 1a event was associated with decreases in CO_2, which was likely due to a combination of factors, including reduced volcanic activity, enhanced continental weathering, carbonate precipitation, and organic C burial (Kashiwagi, 2016; Bauer et al., 2017; Adloff et al., 2020).

OAE 2

Cretaceous OAE 2, also known as the Cenomanian-Turonian extinction and the Bonarelli Event, occurred around 94 million years ago and lasted up to ~900 kyr (Clarkson et al., 2018; Hu et al., 2020) (Table 1). This event was characterized by a rapid increase in atmospheric CO_2 levels, possibly caused by Madagascar and/or Caribbean LIP (Figure 1) (Turgeon and Creaser, 2008), which led to global warming of around 2–10°C (Forster et al., 2007; Huber et al., 2018) and marine anoxia (Clarkson et al., 2018) (Figure 5). This event ultimately caused widespread devastation of marine ecosystems (Coccioni, 2004) and widespread deposition of organic matter (Jenkyns, 2010). The carbon cycle perturbations during the event were globally recorded as a broad positive carbon isotope excursion with a magnitude of around 2–5‰, possibly with an abrupt ~3‰ NCE superimposed on the onset of the PCE (Figure 1) (Kuroda et al., 2007; Jenkyns, 2010; Owens et al., 2013).

In 2011, a modeling study by Flögel et al. utilized a combination of biogeochemical box models (the Cretaceous Ocean Box Model with 27 ocean boxes, COBM) and an Earth system model (known as GENESIS) to investigate the carbon cycle perturbations during the OAE 2 event. The study confirmed that under a volcanic LIP degassing scenario with a $\delta^{13}C$ value of −5‰ (Wallmann, 2001), high productivity and its following organic carbon burial due to increased nutrient supply from continental weathering, could produce a ~2.5‰ PCE (Figure 5), and lead to >90% global deep-ocean anoxia. In addition, Flögel et al. (2011) proposed that C:P ratios probably increased under high CO_2 conditions in a well-ventilated ocean, contributing to ocean anoxia. With a light carbon source with a $\delta^{13}C$ value of −5‰, ~19,000–33,000 Pg C (Table 1) was required for an abrupt ~3‰ NCE, possibly superimposed on the onset of the PCE (Figure 1) in a simple one-box model of the atmosphere–ocean C cycle (Kuroda et al., 2007). The different C isotope patterns produced in these two models probably highlight a significant role of primary productivity (and also varied C:P ratios) in the C cycle of OAE 2 (Flögel et al., 2011).

During OAE 2, the varying C:P ratios were likely caused by increased P supply from land and P recycling back into seawater

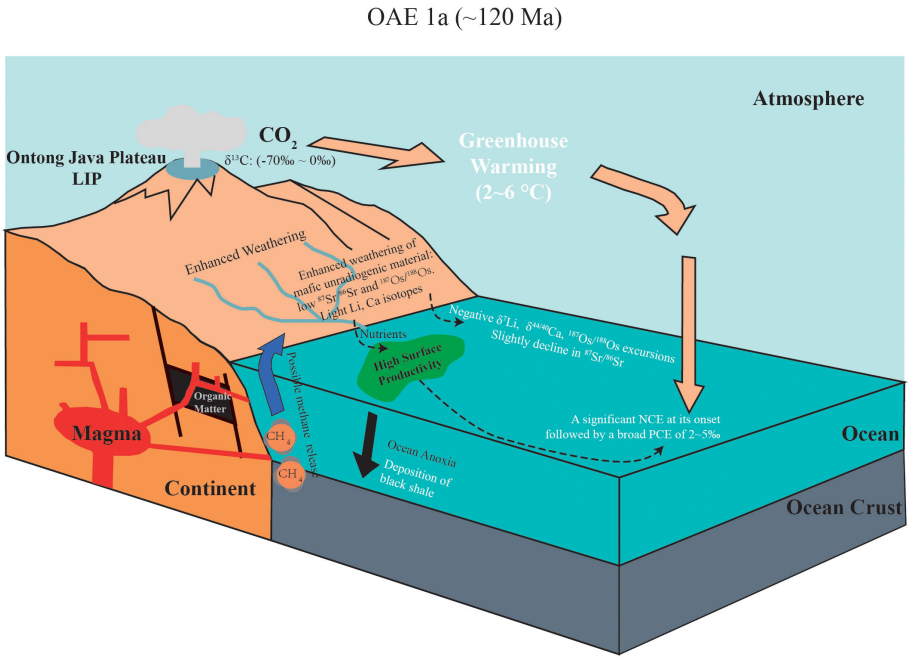

FIGURE 4
Driving mechanisms and environmental impacts of OAE 1a (modified from Hu et al., 2020).

under low oxygen conditions (Nederbragt et al., 2004; Tsandev and Slomp, 2009; Flögel et al., 2011). By applying a box model of oceanic P, C, and O cycles (Slomp and Van Cappellen, 2007), Tsandev and Slomp (2009) argued that oceanic anoxia could be triggered by enhanced continental weathering, which provided more P supply into the ocean. They also suggested that the C-P-O cycle is particularly sensitive to oceanic mixing. Aside from increased weathering P inputs, the oceanic P concentrations can be increased by enhanced benthic (seafloor) regeneration of organic P under anoxic conditions. This can promote primary productivity, and organic C burial, as shown in the cGENIE model (Monteiro et al., 2012), and then generate a rapid 2‰ PCE in coupled C-P models (Nederbragt et al., 2004). Additionally, ocean circulation can influence local primary productivity and organic C burial by changing oxygen availability and nutrient concentrations between ocean basins. Studies using the CESM (Trabucho Alexandre et al., 2010) and a regional ocean circulation model (Topper et al., 2011) have shown this to be the case.

Increases in weathering fluxes were also required in the box modeling of other element cycles, such as Ca, Sr, Os, Li, and S (Blättler et al., 2011; Pogge Von Strandmann et al., 2013; Gomes et al., 2016; Nana Yobo et al., 2021). For example, a threefold increase in weathering flux (Table 2) was required in an oceanic box model of coupled Sr and Ca cycles to explain their behavior during OAE 2 (Blättler et al., 2011). Later, the increased factor was revised to be approximately 1–3 times (Table 2) when the Os and Li isotopic variations during the OAE 2 were also considered in a box model of coupled Li and Os cycles (Pogge Von Strandmann et al., 2013). More recently, box modeling of the increases in seawater $^{87}Sr/^{86}Sr$ suggested a rise of only 1.8 times in the weathering flux of Sr (Table 2), but with a more significant role of enhanced hydrothermal activity in the event (Nana Yobo et al., 2021).

Simple box modeling has also been used to investigate the extent of marine anoxia during OAE 2, particularly through the uranium (U) cycle (Montoya-Pino et al., 2010; Flögel et al., 2011; Clarkson et al., 2018; McDonald et al., 2022). U isotope compositions of seawater ($\delta^{238}U$) were represented in a simple mass-balance equation of the U cycle, to calculate the anoxic area of the ocean sedimentary environment. Here, an increase from a modern value of 0.3% to ~1–2% of the anoxic seafloor was suggested to have occurred during OAE 2 (Montoya-Pino et al., 2010). However, subsequent studies have suggested different extents of marine anoxia during this event. For example, the GENESIS-COBM model proposed an anoxic extent of >90% of the deep ocean (Flögel et al., 2011), while the cGENIE model suggested an extent of >50% of the ocean volume could have been anoxic (Monteiro et al., 2012) (Table 3).

These high estimates were questioned by Owens et al. (2013), who used a forward geochemical box model of C and S cycles and suggested that only ~2.5–5% of global seafloor area (Table 3) was overlain by euxinic waters during the OAE 2 interval. In contrast, a dynamic box model of coupled C, P, and U cycles proposed that ~5–15% anoxia area (Table 3) was required to reproduce the negative $\delta^{238}U$ excursion with the PCE during OAE 2 (Clarkson et al., 2018). Recently, McDonald et al. (2022) revisited the negative U isotope excursion and found a larger magnitude of ~0.9‰, and re-modeled it in a dynamic U box model, which suggested that the anoxic area of the seafloor was only ~21% during the event

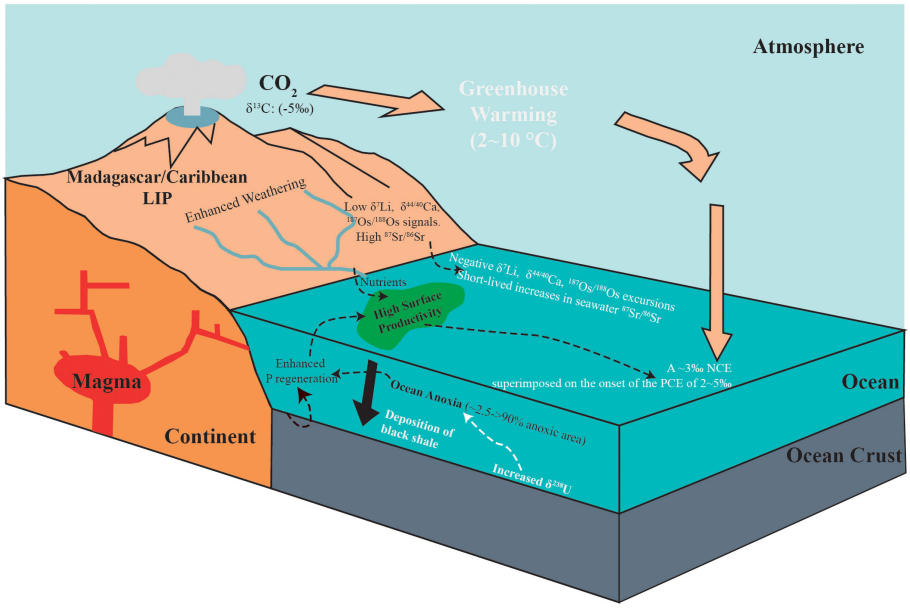

FIGURE 5
Driving mechanisms and environmental impacts of OAE 2 (modified from Hu et al., 2020).

(Table 3). The differences in the U isotope records and indicated anoxic areas indicate that anoxia may differ between ocean regions (Table 3). This is supported by the inconsistent I/Ca ratio records on a global scale and high oxygen availabilities of some regional deep waters simulated in the cGENIE model (Zhou et al., 2015).

The periodicity of redox conditions during the Cretaceous, as suggested by the in-turn development of black shales and red beds during the Cretaceous (Wang et al., 2011), has also been studied using modeling approaches. Handoh and Lenton (2003) noticed periodicities of ~5 Myr in the C, P cycles and seawater redox conditions, and hypothesized it to be a self-sustaining oscillation in response to an increase in the P supply from the land above a critical threshold. By applying a model of coupled C, N, P, and O cycles (a predecessor of the COPSE model), they suggested that the oscillations were primarily maintained by positive feedback between P concentration, biological productivity, and anoxia in the ocean (Handoh and Lenton, 2003). In addition to the long-term oscillation, a distinct short-term redox cyclicity (~1 Myr) was recognized during OAE 2 in iron speciation data (Poulton et al., 2015). In their study, new S isotope data and a simple S isotope box model indicated that fluctuations in the weathering influxes of S and reactive iron due to the dynamic hydrological cycle likely drove this short-term redox cyclicity.

Therefore, phosphorus cycling during OAE 2 likely played a critical role in both the initiation and cessation of ocean anoxia. Organic carbon burial (e.g., Monteiro et al., 2012), as well as enhanced continent weathering (e.g., Pogge Von Strandmann et al., 2013), were both essential processes that contributed to the reduction of atmospheric CO_2 levels (Kashiwagi, 2016), ultimately leading to the termination of the OAE 2 event.

The PETM event

The PETM event (Figure 6), which occurred approximately 56 million years ago and lasted for 150–220 thousand years, saw a global average temperature increase of around 5–8°C (Röhl et al., 2007; McInerney and Wing, 2011; Frieling et al., 2017; Haynes and Hönisch, 2020). The North Atlantic Igneous Province (Figure 1) (Kraus and Riggins, 2007; Gutjahr et al., 2017; Jones et al., 2019) and/or methane clathrate release (Dickens et al., 1995; Dickens, 2011) have been proposed as the causes of the onset of this event, leading to extreme changes in the C cycle. The perturbation of the carbon cycle was recorded as significant NCEs in both marine and terrestrial carbon reservoirs (Koch et al., 1992; Cui et al., 2021a), with magnitudes ranging from −2‰ to −7‰ (Figure 1) (Koch et al., 1992; McInerney and Wing, 2011; Minshull et al., 2016). This event was also associated with profound biological consequences, including the largest mammalian faunal turnover of the Cenozoic (Koch et al., 1992).

The origin of the ^{13}C-depleted carbon source for the PETM event is still a matter of debate. In 1995, a carbon mass balance calculation suggested that a 2–3‰ NCE during the PETM event was likely caused by the thermal dissociation of oceanic CH_4 hydrate with a $\delta^{13}C$ value of −60‰ (Table 1) (Dickens et al., 1995). Later, the rapid burning of accumulated Paleocene terrestrial organic carbon

TABLE 3 Summary of assumed oceanic anoxic extent during OAE 2.

Hyperthermal events	Model or Proxy	Anoxic/Euxinic extent	Reference
OAE 2	U isotope and U box model	~1–2% of seafloor (Anoxic)	Montoya-Pino et al. (2010)
	GENESIS-COBM	>90% of the deep ocean (Anoxic)	Flögel et al. (2011)
	cGENIE	>50% ocean (Anoxic)	Monteiro et al. (2012)
	C and S box model	~2.5–5% of seafloor area (Euxinic)	Owens et al. (2013)
	C, P, and U box model	~8–15% of seafoor area (Anoxic)	Clarkson et al. (2018)
	U box model	~21% of seafloor area (Anoxic)	McDonald et al. (2022)

(Table 1) was proposed as an alternative to releasing gas hydrates to explain the decoupled C and S isotope variations during this interval with a simple box model of the C and S cycles (Kurtz et al., 2003). When seafloor $CaCO_3$ dissolution data during the PETM became available, the cGENIE model was used to match the data and suggested a −22‰ carbon source (~6,800 Pg) (Table 1), possibly a combination of methane, volcanic CO_2, organic matter-derived CO_2 (Panchuk et al., 2008).

However, the methane hypothesis (~1,500–3,000 Pg carbon with a $\delta^{13}C$ value of −50‰) (Table 1) was shown to also reproduce the seafloor $CaCO_3$ dissolution curve and a ~−4‰ NCE in the LOSCAR model (Zeebe et al., 2009; Frieling et al., 2016). Similarly, a combined ~900–1,400 Pg of carbon as CO_2 and CH_4 (Table 1) was shown to drive the observed $\delta^{13}C$ excursion and global warming of 3°C in a global C cycle box model coupled with an atmospheric CH_4 box (Carozza et al., 2011). However, the cGENIE model (Cui et al., 2011) required at least double the amount of CH_4 (Table 1) for isotopic mass balance since most of the released methane remains in the sediments, as shown in a thermohydraulic model (Minshull et al., 2016).

Seawater pH variations indicated from B isotope data were then used together with carbon isotopes to constrain the carbon source in the cGENIE model (Gutjahr et al., 2017), showing that a volcanic-dominant C source of −11‰ to −17‰ (isotopically heavier than previously considered) (Table 1) was likely related to the North Atlantic Igneous Province, although records of Hg enrichment in sediments suggest that volcanism did not provide all of the carbon input (Kender et al., 2021). An abrupt input of an isotopically-light carbon source (−35‰) combined with elevated volcanic outgassing (−6‰) could also satisfy the constraint of C isotopes, pH, and temperatures in the cGENIE model (Kirtland Turner, 2018). Recent box modeling of the C cycle suggested a carbon source of −22‰ (Table 1) based on new C isotope data from biomarkers (Cui et al., 2021a). In conclusion, the C composition and input amounts during the PETM event are still sources of debate (Table 1).

Simulations using various box models and 3D Earth system models have suggested possible environmental outcomes of the PETM event. Examples are listed here in order of modeling complexity from more simple to more complex. A simple box model of the Li cycle was applied to study the observed negative δ^7Li excursion, suggesting enhanced continent weathering during the PETM event (Pogge Von Strandmann et al., 2021). Earth system models with intermediate complexity (represented by the cGENIE model) have proposed globally enhanced calcite burial (or deepening of the calcite compensation depth) (Penman et al., 2016), enhanced organic burial (Gutjahr et al., 2017), enhanced ocean stratification (Kirtland Turner et al., 2017), and ocean deoxygenation (Remmelzwaal et al., 2019) (Figure 6). Earth system models with higher complexity, such as CESM, have also been used to study the climate impact of the PETM event, revealing significant changes in hydroclimate such as extreme precipitation (Rush et al., 2021; Shields et al., 2021) and increased surface seawater temperature (Frieling et al., 2017) due to increased CO_2. Hydroclimate responses simulated in the Hadley Centre Atmosphere-Ocean General Circulation Model (HadCM3L), were suggested to be heterogeneous, meaning precipitation-evaporation increased in some regions but decreased in others (Carmichael et al., 2017). These impacts on climate or environment, particularly enhanced organic carbon and carbonate burial, acted as negative feedbacks on the increased CO_2 and temperature, ultimately contributing to the termination of the PETM event (e.g., Kurtz et al., 2003; Penman et al., 2016).

Short summaries and comparisons of hyperthermal events

Plentiful modeling studies, as well as proxy records, have suggested that the Mesozoic-Paleogene hyperthermal events were caused by vast emissions of ^{13}C-depleted carbon into the atmosphere and ocean. The proposed composition of carbon emissions that triggered these hyperthermal events varies significantly for a specific hyperthermal event or among these hyperthermal events: $\delta^{13}C$ values are in the range of −60 to −5‰ for the PTB event, of −60 to −6‰ for TOAE, of −70 to 0‰ for OAE 1a, −5‰ for OAE 2, of −60 to −11‰ for the PETM event, respectively (Table 1). Whereas their amount of carbon emissions is in the range of 900–450,000 Pg C (Table 1). We find that the light carbon source that drove the PETM event is believed to have huge contributions from organic carbon or methane (Dickens et al., 1995; Panchuk et al., 2008; Zeebe et al., 2009; Carozza et al., 2011; Cui et al., 2011; Gutjahr et al., 2017; Cui et al., 2021a), and the carbon source for OAE 2 is probably from a volcanic CO_2 source (Kuroda et al., 2007; Flögel et al., 2011). Besides the PETM and OAE 2, the assumed carbon sources for other hyperthermal events range from

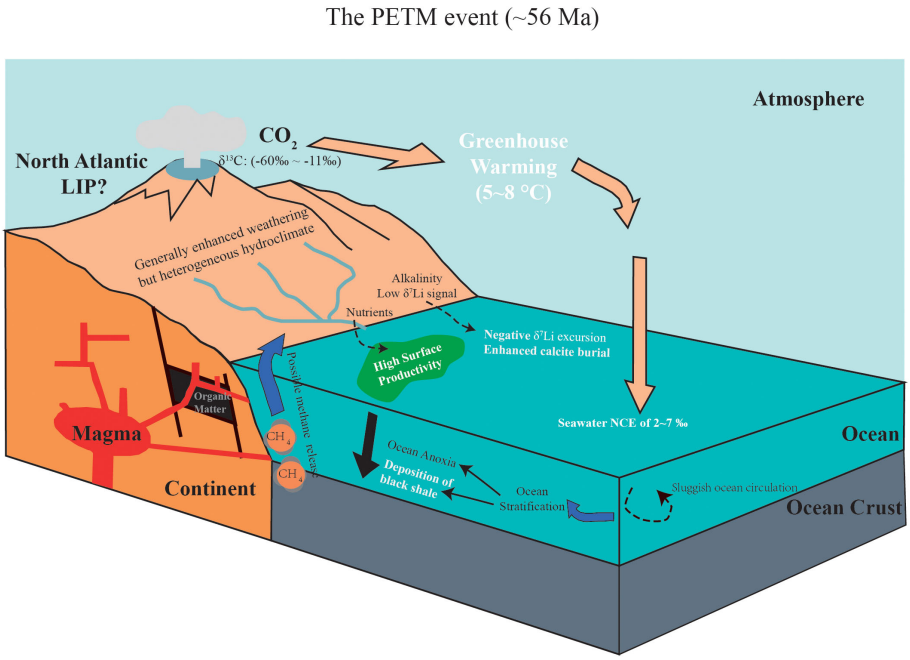

FIGURE 6
Driving mechanisms and environmental impacts of the PETM event (modified from Hu et al., 2020).

volcanic sources to organic matter and methane-derived carbon (e.g., Adloff et al., 2020). The shortest onset duration (8–23 kyr) for warming 5–8°C during the PETM event (Hu et al., 2020) likely explains the necessity of involving a carbon source with a $\delta^{13}C$ value lighter than volcanic sources (< −5‰) for the PETM event. More detailed duration and warming magnitudes comparisons refer to Hu et al. (2020).

In addition, both models and proxy records have shown the biogeochemical consequences of warming, including but not limited to intensified continental weathering, ocean anoxia, and acidification. However, their exact magnitudes are still subject to debate. Enhanced continent weathering is an important and necessary precondition (Table 2) to respond to high CO_2 conditions and to replicate the isotope records (i.e., negative $\delta^{44}/^{40}Ca$ and $\delta^{7}Li$ excursions) (e.g., Lechler et al., 2015; Sun et al., 2018), although the radiogenic isotopes (Sr and Os) might show different behaviors among hyperthermal events likely due to the different level of eruptions of LIPs and their weathering and different hypothermal intensity (Pogge Von Strandmann et al., 2013; Them et al., 2017b). Given different box models of different combined element cycles applied, the proposed enhanced weathering factor ranges from 1.5 to 18 times for these hyperthermal events (Table 2). Considering that these simple box models generally lack the constraints from the carbon cycle, combing them with Earth system box models or 3D Earth system models is promising to further quantify the weathering process during each hyperthermal event.

Modeling studies also suggest global warming could lead to ocean anoxia due to lower oxygen solubility, weaker ocean circulation (e.g., Penn et al., 2018), and likely higher surface productivity that produces more organic matter consuming oxygen in deeper seawater (e.g., Monteiro et al., 2012). However, quantifying the extent of ocean anoxia is still subject to modeling and proxy efforts since the exact extent of ocean anoxia is still unknown for all hyperthermal events. For instance, the assumed anoxic extent ranges significantly from ~1–2% to >90% of the global seafloor area (Montoya-Pino et al., 2010; Flögel et al., 2011; Owens et al., 2013) during OAE 2 (Table 3). Meanwhile, compared with OAE 2, the quantitative estimates of ocean anoxia for other hyperthermal events lack, which requires more proxy and modeling efforts.

Previous studies have classified these hyperthermal events into two types based on seawater carbon isotope characteristics (Hu et al., 2020). One type of hyperthermal event (PTB, TOAE, and PETM) generally shows an NCE pattern, and the other type (OAE 1a and OAE 2) exhibits PCE possibly with an abrupt NCE at its onset (Figure 1). However, the C isotope pattern for these hyperthermal events requires further global stratigraphic correlation work to verify. For example, whether an abrupt NCE exists at the onset of OAE 2 is uncertain. In contrast to an NCE record at the initial part of the PCE of OAE 2 from Bonarelli of Western Tethys (Kuroda et al., 2007), the C isotope profile from the Gongzha of Southern Tibet lacks an NCE at the onset of PCE (Hu et al., 2020). In addition, other seawater carbon variations prior to or after the hyperthermal event may also interfere with the identification of the C isotope variation pattern for each hyperthermal event, such as a PCE prior to the NCE of PETM (Hu et al., 2020; Wang et al., 2022). Future stratigraphic correlation works are expected to help address these uncertainties in identifying seawater C isotope patterns.

The hyperthermal events of PCE have been previously considered to be triggered by volcanism associated with LIPs in the deep-sea environment, while the NCE type was initiated by LIPs

on land (Hu et al., 2020). However, this theoretical hypothesis requires further modeling verifications. As far as the current modeling work suggests, vast emissions of ^{13}C-depleted carbon into the atmosphere and ocean would drive a (short-term) NCE in seawater (e.g., Kuroda et al., 2007), while the enhanced weathering input of nutrients and regeneration of P from the seafloor promoted surface productivity and organic carbon burial in anoxic ocean, ultimately resulting in a (relatively broad) PCE record (e.g., Flögel et al., 2011; Chen et al., 2022). Therefore, we propose that the different responses of seawater carbon isotope patterns among hyperthermal events likely result from interactions between the light carbon input and increased organic carbon burial. In other words, interactions between the light carbon emission pattern (i.e., carbon source, carbon emission rate, and total carbon emission) and the extent of primary productivity and organic carbon burial largely determine the seawater C isotope response pattern to the warming event.

To summarize, the development of simple box models, Earth system box models, and 3D Earth system models progressed in tandem with the increasing availability of proxy constraints, with a focus on the composition and amount of carbon emission that triggered these hyperthermal events (Table 1), and on the biogeochemical consequences of warming (Tables 2, 3). However, the exact amplitude of environmental impact is still debated and requires further modeling and proxy efforts. In addition, the mechanism that terminated the warming has been neglected in the previous modeling works.

Simulating hyperthermal events in long-term climate-biogeochemical models

To date, the models used to study hyperthermal events span from simple single-element box models, and Earth system box models (e.g., LOSCAR, COPSE), to complex 3D spatially-resolved models. These models have provided valuable insights into the drivers and potential impacts of these hyperthermal events, but they have limitations and uncertainties. The simple box models or Earth system box models do not capture the spatial resolution and full complexity of the Earth system and its feedback mechanisms, meaning that geological processes, particularly weathering processes, are very poorly represented within them (e.g., Goddéris et al., 2014). The weathering of LIPs during hyperthermal events, which is crucial in reducing the increased atmospheric CO_2 (e.g., Pogge Von Strandmann et al., 2013; Them et al., 2017b), has been chiefly modeled in box models, but they do not account for the spatial variations in temperature, runoff, and topography, which are essential factors influencing the weathering process.

On the other hand, the 3D Earth system models are computationally expensive and have limitations in terms of the simulated timescale – they cannot be integrated across the whole duration of most of the events discussed. A compromise between these approaches can be made with so-called 'semi-spatial' Earth system models. These models use data structures of steady-state 3D climate model simulations to represent continental surface processes in 3D while the ocean is represented by a box model. The first of these models to be developed was GEOCLIM (Donnadieu et al., 2006), which can run up to around 10 Myr – limited by the changing continental configuration. It has been applied to hyperthermal events by producing predictions over long >100 kyr timescales for the Deccan Traps warming at the K–Pg boundary, combining the LIP warming with the bolide impact event (Le Hir et al., 2020).

A new semi-spatial model is the Spatial-Continuous Integration 'SCION' model (Mills et al., 2021; Zhang et al., 2023). It uses the same climate model data structure as GEOCLIM but interpolates this over geological time to run continuously over the 539 million years of the Phanerozoic Eon. This allows for extensive model validation against multiple environmental datasets (atmospheric CO_2, atmospheric O_2, marine SO_4) and isotope proxies ($\delta^{13}C$, $\delta^{34}S$, $^{87}Sr/^{86}Sr$), and therefore provides a relatively robust background model setup for simulating a hyperthermal event (e.g., CO_2 level, marine phosphate level, marine productivity, background CO_2 degassing rate) that closely aligns with the Phanerozoic-scale geological record.

Models like SCION and GEOCLIM are currently under-utilized for exploring hyperthermal events and could help tie together the long-term but more poorly-constrained experiments in simple box models or Earth system box models, with the detailed but shorter-term experiments in 3D models. For example, SCION has been used to test the interplay between CO_2 degassing and LIP weathering in controlling climate over the Columbia River Basalt emplacement (Longman et al., 2022). These types of simulations that include long-term continental and marine processes may help us better understand these events – particularly concerning what terminates a hyperthermal event. Event termination is currently under-explored compared to the initiation, given that 3D Earth system models typically cannot run to the full duration of the event, which could last up to millions of years (e.g., for the PTB-Early Triassic hyperthermal; Sun et al., 2018; Wu et al., 2021).

Conclusions

Numerous simulation studies have been conducted to investigate the mechanisms of hyperthermal events. When summarizing the existing modeling work on the Mesozoic-Paleogene hyperthermal events, it can be observed that: 1) the developments of simple box models, Earth system box models, and 3D Earth system models have progressed in tandem with the increasing availability of proxy constraints, 2) the biogeochemical consequences of warming, including but not limited to intensified continental weathering, ocean anoxia, and acidification, have been widely acknowledged in both models and proxy records, but their exact magnitudes and drivers are still subject to debate and require further modeling and proxy efforts, 3) determining the composition and amount of carbon emissions that triggered these hyperthermal events also demands additional modeling and proxy constraints. Semi-spatial models like SCION and GEOCLIM may help to bridge the gap between complex 3D representations of continental processes and long timescales of geological records, potentially

offering fresh insights and perspectives on the drivers of, and biogeochemical responses to, hyperthermal events.

Author contributions

YZ: Conceptualization; Investigation; Writing – original draft; Writing – review & editing; BM: Conceptualization; Funding acquisition; Supervision; Writing – review & editing; TH: Conceptualization; Supervision; Writing – review & editing; XH: Supervision; Writing – review & editing; MZ: Conceptualization; Funding acquisition; Supervision. All authors contributed to the article and approved the submitted version.

Funding

This research was financially supported by the National Natural Science Foundation of China (41888101 and 41921002), the China Postdoctoral Science Foundation (2023M733592), and the Jiangsu Funding Program for Excellent Postdoctoral Talent. BM's contribution was supported by the UK Natural Environment Research Council (NE/S009663/1 and NE/X011208/1).

Acknowledgments

This manuscript contributes to the Integrated Understanding of the Early Jurassic Earth System and Timescale (JET) project and the IGCP 739 project.

Conflict of interest

The authors declare that the research was conducted in the absence of any commercial or financial relationships that could be construed as a potential conflict of interest.

The reviewer SJ declared a shared affiliation with the author TH to the handling editor at time of review.

Publisher's note

References

Adloff, M., Greene, S. E., Parkinson, I. J., Naafs, B. D. A., Preston, W., Ridgwell, A., et al. (2020). Unravelling the sources of carbon emissions at the onset of Oceanic Anoxic Event (OAE) 1a. *Earth Planetary Sci. Lett.* 530, 115947. doi: 10.1016/j.epsl.2019.115947

Algeo, T. J., Luo, G. M., Song, H. Y., Lyons, T. W., and Canfield, D. E. (2015). Reconstruction of secular variation in seawater sulfate concentrations. *Biogeosciences* 12, 2131–2151. doi: 10.5194/bg-12-2131-2015

Ando, A., Kaiho, K., Kawahata, H., and Kakegawa, T. (2008). Timing and magnitude of early Aptian extreme warming: Unraveling primary $\delta^{18}O$ variation in indurated pelagic carbonates at Deep Sea Drilling Project Site 463, central Pacific Ocean. *Palaeogeography Palaeoclimatology Palaeoecol.* 260, 463–476. doi: 10.1016/j.palaeo.2007.12.007

Baroni, I. R., Pohl, A., van Helmond, N. A. G. M., Papadomanolaki, N. M., Coe, A. L., Cohen, A. S., et al. (2018). Ocean circulation in the toarcian (Early jurassic): A key control on deoxygenation and carbon burial on the European shelf. *Paleoceanography Paleoclimatology* 33, 994–1012. doi: 10.1029/2018PA003394

Bauer, K. W., Bottini, C., Katsev, S., Jellinek, M., Francois, R., Erba, E., et al. (2022). Ferruginous oceans during OAE1a and collapse of the marine sulfate pool. *Earth Planetary Sci. Lett.* 578, 117324. doi: 10.1016/j.epsl.2021.117324

Bauer, K. W., Zeebe, R. E., and Wortmann, U. G. (2017). Quantifying the volcanic emissions which triggered Oceanic Anoxic Event 1a and their effect on ocean acidification. *Sedimentology* 64, 204–214. doi: 10.1111/sed.12335

Bergman, N. M., Lenton, T. M., and Watson, A. J. (2004). COPSE: A new model of biogeochemical cycling over phanerozoic time. *Am. J. Sci.* 304, 397–437. doi: 10.2475/ajs.304.5.397

Berner, R. A., and Kothavala, Z. (2001). Geocarb III: A revised model of atmospheric CO_2 over phanerozoic time. *Am. J. Sci.* 301, 182–204. doi: 10.2475/ajs.301.2.182

Bjerrum, C. J., Surlyk, F., Callomon, J. H., and Slingerland, R. L. (2001). Numerical paleoceanographic study of the Early Jurassic Transcontinental Laurasian Seaway. *Paleoceanography* 16, 390–404. doi: 10.1029/2000PA000512

Blättler, C. L., Jenkyns, H. C., Reynard, L. M., and Henderson, G. M. (2011). Significant increases in global weathering during Oceanic Anoxic Events 1a and 2 indicated by calcium isotopes. *Earth Planetary Sci. Lett.* 309, 77–88. doi: 10.1016/j.epsl.2011.06.029

Brazier, J.-M., Suan, G., Tacail, T., Simon, L., Martin, J. E., Mattioli, E., et al. (2015). Calcium isotope evidence for dramatic increase of continental weathering during the Toarcian oceanic anoxic event (Early Jurassic). *Earth Planetary Sci. Lett.* 411, 164–176. doi: 10.1016/j.epsl.2014.11.028

Carmichael, M. J., Inglis, G. N., Badger, M. P. S., Naafs, B. D. A., Behrooz, L., Remmelzwaal, S., et al. (2017). Hydrological and associated biogeochemical consequences of rapid global warming during the Paleocene-Eocene Thermal Maximum. *Global Planetary Change* 157, 114–138. doi: 10.1016/j.gloplacha.2017.07.014

Carozza, D. A., Mysak, L. A., and Schmidt, G. A. (2011). Methane and environmental change during the Paleocene-Eocene thermal maximum (PETM): Modeling the PETM onset as a two-stage event. *Geophysical Res. Lett.* 38, L05702. doi: 10.1029/2010GL046038

Chen, X., Guo, H., Yao, H., Han, K., and Wang, H. (2022). Processes and forcing mechanisms ofthe carbon cycle perturbation during Cretaceous Oceanic Anoxic Event 2 (in Chinese with English abstract). *Chin. Sci. Bull.* 67, 1677–1688. doi: 10.1360/TB-2021-0806

Clarkson, M. O., Kasemann, S. A., Wood, R. A., Lenton, T. M., Daines, S. J., Richoz, S., et al. (2015). Ocean acidification and the Permo-Triassic mass extinction. *Science* 348, 229–232. doi: 10.1126/science.aaa0193

Clarkson, M. O., Stirling, C. H., Jenkyns, H. C., Dickson, A. J., Porcelli, D., Moy, C. M., et al. (2018). Uranium isotope evidence for two episodes of deoxygenation during Oceanic Anoxic Event 2. *Proc. Natl. Acad. Sci.* 115, 2918–2923. doi: 10.1073/pnas.1715278115

Coccioni, R. (2004). Planktonic foraminifera and environmental changes across the Bonarelli event (OAE 2, latest Cenomanian) in its type area: A high-resolution study from the Tethyan reference Bottaccione section (Gubbio, Central Italy). *J. Foraminiferal Res.* 34, 109–129. doi: 10.2113/0340109

Cui, Y., Diefendorf, A. F., Kump, L. R., Jiang, S., and Freeman, K. H. (2021a). Synchronous marine and terrestrial carbon cycle perturbation in the high arctic during the PETM. *Paleoceanography Paleoclimatology* 36, e2020PA003942. doi: 10.1029/2020PA003942

Cui, Y., Kump, L. R., Ridgwell, A. J., Charles, A. J., Junium, C. K., Diefendorf, A. F., et al. (2011). Slow release of fossil carbon during the Palaeocene-Eocene thermal maximum. *Nat. Geosci.* 4, 481–485. doi: 10.1038/ngeo1179

Cui, Y., Li, M., van Soelen, E. E., and Peterse, F. (2021b). Massive and rapid predominantly volcanic CO_2 emission during the end-Permian mass extinction. *Proc. Natl. Acad. Sci.* 118, e2014701118. doi: 10.1073/pnas.2014701118

Dal Corso, J., Mills, B. J. W., Chu, D., Newton, R. J., Mather, T. A., Shu, W., et al. (2020). Permo–Triassic boundary carbon and mercury cycling linked to terrestrial ecosystem collapse. *Nat. Commun.* 11, 2962. doi: 10.1038/s41467-020-16725-4

Dal Corso, J., Song, H., Callegaro, S., Chu, D., Sun, Y., Hilton, J., et al. (2022). Environmental crises at the Permian–Triassic mass extinction. *Nat. Rev. Earth Environ.* 3, 197–214. doi: 10.1038/s43017-021-00259-4

Dera, G., and Donnadieu, Y. (2012). Modeling evidences for global warming, Arctic seawater freshening, and sluggish oceanic circulation during the Early Toarcian anoxic event. *Paleoceanography* 27, PA2211. doi: 10.1029/2012PA002283

Dickens, G. R. (2011). Down the Rabbit Hole: toward appropriate discussion of methane release from gas hydrate systems during the Paleocene-Eocene thermal maximum and other past hyperthermal events. *Climate Past* 7, 831–846. doi: 10.5194/cp-7-831-2011

Dickens, G. R., O'Neil, J. R., Rea, D. K., and Owen, R. M. (1995). Dissociation of oceanic methane hydrate as a cause of the carbon isotope excursion at the end of the Paleocene. *Paleoceanography* 10, 965–971. doi: 10.1029/95PA02087

Di Lucia, M., Trecalli, A., Mutti, M., and Parente, M. (2012). Bio-chemostratigraphy of the Barremian-Aptian shallow-water carbonates of the southern Apennines (Italy): pinpointing the OAE1a in a Tethyan carbonate platform. *Solid Earth* 3, 1–28. doi: 10.5194/se-3-1-2012

Donnadieu, Y., Goddéris, Y., Pierrehumbert, R., Dromart, G., Jacob, R., and Fluteau, F. (2006). A GEOCLIM simulation of climatic and biogeochemical consequences of Pangea breakup. *Geochemistry Geophysics Geosystems* 7, Q11019. doi: 10.1029/2006GC001278

Flögel, S., Wallmann, K., Poulsen, C. J., Zhou, J., Oschlies, A., Voigt, S., et al. (2011). Simulating the biogeochemical effects of volcanic CO_2 degassing on the oxygen-state of the deep ocean during the Cenomanian/Turonian Anoxic Event (OAE2). *Earth Planetary Sci. Lett.* 305, 371–384. doi: 10.1016/j.epsl.2011.03.018

Forster, A., Schouten, S., Moriya, K., Wilson, P. A., and Sinninghe Damsté, J. S. (2007). Tropical warming and intermittent cooling during the Cenomanian/Turonian Oceanic Anoxic Event 2: Sea surface temperature records from the equatorial Atlantic. *Paleoceanography* 22, PA1219. doi: 10.1029/2006PA001349

Frieling, J., Gebhardt, H., Huber, M., Adekeye, O. A., Akande, S. O., Reichart, G.-J., et al. (2017). Extreme warmth and heat-stressed plankton in the tropics during the Paleocene-Eocene Thermal Maximum. *Sci. Adv.* 3, e1600891. doi: 10.1126/sciadv.1600891

Frieling, J., Svensen, H. H., Planke, S., Cramwinckel, M. J., Selnes, H., and Sluijs, A. (2016). Thermogenic methane release as a cause for the long duration of the PETM. *Proc. Natl. Acad. Sci.* 113, 12059–12064. doi: 10.1073/pnas.1603348113

Gill, B. C., Lyons, T. W., and Jenkyns, H. C. (2011). A global perturbation to the sulfur cycle during the Toarcian Oceanic Anoxic Event. *Earth Planetary Sci. Lett.* 312, 484–496. doi: 10.1016/j.epsl.2011.10.030

Goddéris, Y., Donnadieu, Y., Le Hir, G., Lefebvre, V., and Nardin, E. (2014). The role of palaeogeography in the Phanerozoic history of atmospheric CO_2 and climate. *Earth-Science Rev.* 128, 122–138. doi: 10.1016/j.earscirev.2013.11.004

Gomes, M. L., Hurtgen, M. T., and Sageman, B. B. (2016). Biogeochemical sulfur cycling during Cretaceous oceanic anoxic events: A comparison of OAE1a and OAE2. *Paleoceanography* 31, 233–251. doi: 10.1002/2015PA002869

Grard, A., François, L. M., Dessert, C., Dupré, B., and Goddéris, Y. (2005). Basaltic volcanism and mass extinction at the Permo-Triassic boundary: Environmental impact and modeling of the global carbon cycle. *Earth Planetary Sci. Lett.* 234, 207–221. doi: 10.1016/j.epsl.2005.02.027

Grasby, S. E., Beauchamp, B., and Knies, J. (2016). Early Triassic productivity crises delayed recovery from world's worst mass extinction. *Geology* 44, 779–782. doi: 10.1130/G38141.1

Gutjahr, M., Ridgwell, A., Sexton, P. F., Anagnostou, E., Pearson, P. N., Pälike, H., et al. (2017). Very large release of mostly volcanic carbon during the Palaeocene–Eocene Thermal Maximum. *Nature* 548, 573–577. doi: 10.1038/nature23646

Han, Z., Hu, X., He, T., Newton, R. J., Jenkyns, H. C., Jamieson, R. A., et al. (2022). Early Jurassic long-term oceanic sulfur-cycle perturbations in the Tibetan Himalaya. *Earth Planetary Sci. Lett.* 578, 117261. doi: 10.1016/j.epsl.2021.117261

Handoh, I. C., and Lenton, T. M. (2003). Periodic mid-Cretaceous oceanic anoxic events linked by oscillations of the phosphorus and oxygen biogeochemical cycles. *Global Biogeochemical Cycles* 17, 1–11. doi: 10.1029/2003gb002039

Haynes, L. L., and Hönisch, B. (2020). The seawater carbon inventory at the Paleocene–Eocene Thermal Maximum. *Proc. Natl. Acad. Sci.* 117, 24088–24095. doi: 10.1073/pnas.2003197117

Hesselbo, S. P., Gröcke, D. R., Jenkyns, H. C., Bjerrum, C. J., Farrimond, P., Morgans Bell, H. S., et al. (2000). Massive dissociation of gas hydrate during a Jurassic oceanic anoxic event. *Nature* 406, 392–395. doi: 10.1038/35019044

Hu, X., Li, J., Han, Z., and Li, Y. (2020). Two types of hyperthermal events in the Mesozoic-Cenozoic: Environmental impacts, biotic effects, and driving mechanisms. *Sci. China Earth Sci.* 63, 1041–1058. doi: 10.1007/s11430-019-9604-4

Huber, B. T., MacLeod, K. G., Watkins, D. K., and Coffin, M. F. (2018). The rise and fall of the Cretaceous Hot Greenhouse climate. *Global Planetary Change* 167, 1–23. doi: 10.1016/j.gloplacha.2018.04.004

IPCC (2022). *Global Warming of 1.5°C: IPCC Special Report on Impacts of Global Warming of 1.5°C above Pre-industrial Levels in Context of Strengthening Response to Climate Change, Sustainable Development, and Efforts to Eradicate Poverty. 1st ed* (Cambridge University Press). doi: 10.1017/9781009157940

Jenkyns, H. C. (2010). Geochemistry of oceanic anoxic events. *Geochemistry Geophysics Geosystems* 11, Q03004. doi: 10.1029/2009GC002788

Joachimski, M., Alekseev, A., Grigoryan, A., and Gatovsky, Y. A. (2020). Siberian Trap volcanism, global warming and the Permian-Triassic mass extinction: New insights from Armenian Permian-Triassic sections. *GSA Bull.* 132, 427–443. doi: 10.1130/B35108.1

Jones, S. M., Hoggett, M., Greene, S. E., and Dunkley Jones, T. (2019). Large Igneous Province thermogenic greenhouse gas flux could have initiated Paleocene-Eocene Thermal Maximum climate change. *Nat. Commun.* 10, 5547. doi: 10.1038/s41467-019-12957-1

Kashiwagi, H. (2016). Atmospheric carbon dioxide and climate change since the Late Jurassic (150Ma) derived from a global carbon cycle model. *Palaeogeography Palaeoclimatology Palaeoecol.* 454, 82–90. doi: 10.1016/j.palaeo.2016.04.002

Keller, C. E., Hochuli, P. A., Weissert, H., Bernasconi, S. M., Giorgioni, M., and Garcia, T. I. (2011). A volcanically induced climate warming and floral change preceded the onset of OAE1a (Early Cretaceous). *Palaeogeography Palaeoclimatology Palaeoecol.* 305, 43–49. doi: 10.1016/j.palaeo.2011.02.011

Kender, S., Bogus, K., Pedersen, G. K., Dybkjær, K., Mather, T. A., Mariani, E., et al. (2021). Paleocene/Eocene carbon feedbacks triggered by volcanic activity. *Nat. Commun.* 12, 5186. doi: 10.1038/s41467-021-25536-0

Kirtland Turner, S. (2018). Constraints on the onset duration of the Paleocene–Eocene Thermal Maximum. *Philos. Trans. R. Soc. A: Mathematical Phys. Eng. Sci.* 376, 20170082. doi: 10.1098/rsta.2017.0082

Kirtland Turner, S., Hull, P. M., Kump, L. R., and Ridgwell, A. (2017). A probabilistic assessment of the rapidity of PETM onset. *Nat. Commun.* 8, 353. doi: 10.1038/s41467-017-00292-2

Koch, P. L., Zachos, J. C., and Gingerich, P. D. (1992). Correlation between isotope records in marine and continental carbon reservoirs near the Palaeocene/Eocene boundary. *Nature* 358, 319–322. doi: 10.1038/358319a0

Kraus, M. J., and Riggins, S. (2007). Transient drying during the Paleocene–Eocene Thermal Maximum (PETM): Analysis of paleosols in the bighorn basin, Wyoming. *Palaeogeography Palaeoclimatology Palaeoecol.* 245, 444–461. doi: 10.1016/j.palaeo.2006.09.011

Kump, L. R., and Arthur, M. A. (1999). Interpreting carbon-isotope excursions: Carbonates and organic matter. *Chem. Geology* 161, 181–198. doi: 10.1016/S0009-2541(99)00086-8

Kuroda, J., Ogawa, N. O., Tanimizu, M., Coffin, M. F., Tokuyama, H., Kitazato, H., et al. (2007). Contemporaneous massive subaerial volcanism and late cretaceous Oceanic Anoxic Event 2. *Earth Planetary Sci. Lett.* 256, 211–223. doi: 10.1016/j.epsl.2007.01.027

Kurtz, A. C., Kump, L. R., Arthur, M. A., Zachos, J. C., and Paytan, A. (2003). Early Cenozoic decoupling of the global carbon and sulfur cycles. *Paleoceanography* 18, 1090. doi: 10.1029/2003PA000908

Lechler, M., Pogge von Strandmann, P. A. E., Jenkyns, H. C., Prosser, G., and Parente, M. (2015). Lithium-isotope evidence for enhanced silicate weathering during OAE 1a (Early Aptian Selli event). *Earth Planetary Sci. Lett.* 432, 210–222. doi: 10.1016/j.epsl.2015.09.052

Le Hir, G., Fluteau, F., Suchéras-Marx, B., and Goddéris, Y. (2020). 'Amplifying factors leading to the collapse of primary producers during the Chicxulub impact and Deccan Traps eruptions,' in *Mass Extinctions, Volcanism, and Impacts: New Developments* (Boulder, Colorado, USA: Geological Society of America), 223–245. doi: 10.1130/2020.2544(09)

Lenton, T. M., Daines, S. J., and Mills, B. J. W. (2018). COPSE reloaded: An improved model of biogeochemical cycling over Phanerozoic time. *Earth-Science Rev.* 178, 1–28. doi: 10.1016/j.earscirev.2017.12.004

Longman, J., Mills, B. J. W., Donnadieu, Y., and Goddéris, Y. (2022). Assessing volcanic controls on Miocene climate change. *Geophysical Res. Lett.* 49, e2021GL096519. doi: 10.1029/2021gl096519

Matsumoto, H., Coccioni, R., Frontalini, F., Shirai, K., Jovane, L., Trindade, R., et al. (2022). Mid-Cretaceous marine Os isotope evidence for heterogeneous cause of oceanic anoxic events. *Nat. Commun.* 13, 239. doi: 10.1038/s41467-021-27817-0

McDonald, B. S., Partin, C. A., Sageman, B., and Holmden, C. (2022). Uranium isotope reconstruction of ocean deoxygenation during OAE 2 hampered by uncertainties in fractionation factors and local U-cycling. *Geochimica Cosmochimica Acta* 331, 143–164. doi: 10.1016/j.gca.2022.05.010

McElwain, J. C., Wade-Murphy, J., and Hesselbo, S. P. (2005). Changes in carbon dioxide during an oceanic anoxic event linked to intrusion into Gondwana coals. *Nature* 435, 479–482. doi: 10.1038/nature03618

McInerney, F. A., and Wing, S. L. (2011). The paleocene-eocene thermal maximum: A perturbation of carbon cycle, climate, and biosphere with implications for the future. *Annu. Rev. Earth Planetary Sci.* 39, 489–516. doi: 10.1146/annurev-earth-040610-133431

Meyer, K. M., Yu, M., Jost, A. B., Kelley, B. M., and Payne, J. L. (2011). $\delta^{13}C$ evidence that high primary productivity delayed recovery from end-Permian mass extinction. *Earth Planetary Sci. Lett.* 302, 378–384. doi: 10.1016/j.epsl.2010.12.033

Mills, B. J. W., Donnadieu, Y., and Goddéris, Y. (2021). Spatial continuous integration of Phanerozoic global biogeochemistry and climate. *Gondwana Res.* 100, 73–86. doi: 10.1016/j.gr.2021.02.011

Minshull, T. A., Marín-Moreno, H., Armstrong McKay, D. I., and Wilson, P. A. (2016). Mechanistic insights into a hydrate contribution to the Paleocene-Eocene carbon cycle perturbation from coupled thermohydraulic simulations. *Geophysical Res. Lett.* 43, 8637–8644. doi: 10.1002/2016GL069676

Monteiro, F. M., Pancost, R. D., Ridgwell, A., and Donnadieu, Y. (2012). Nutrients as the dominant control on the spread of anoxia and euxinia across the Cenomanian-Turonian oceanic anoxic event (OAE2): model-data comparison. *Paleoceanography* 27, PA4209. doi: 10.1029/2012PA002351

Montoya-Pino, C., Weyer, S., Anbar, A. D., Pross, J., Oschmann, W., van de Schootbrugge, B., et al. (2010). Global enhancement of ocean anoxia during Oceanic Anoxic Event 2: A quantitative approach using U isotopes. *Geology* 38, 315–318. doi: 10.1130/G30652.1

Nana Yobo, L., Brandon, A. D., Holmden, C., Lau, K. V., and Eldrett, J. (2021). Changing inputs of continental and submarine weathering sources of Sr to the oceans during OAE 2. *Geochimica Cosmochimica Acta* 303, 205–222. doi: 10.1016/j.gca.2021.03.013

Nederbragt, A. J., Thurow, Jü., Vonhof, H., and Brumsack, H.-J. (2004). Modelling oceanic carbon and phosphorus fluxes: implications for the cause of the late Cenomanian Oceanic Anoxic Event (OAE2). *JGS* 161, 721–728. doi: 10.1144/0016-764903-075

Owens, J. D., Gill, B. C., Jenkyns, H. C., Bates, S. M., Severmann, S., Kuypers, M. M. M., et al. (2013). Sulfur isotopes track the global extent and dynamics of euxinia during Cretaceous Oceanic Anoxic Event 2. *Proc. Natl. Acad. Sci.* 110, 18407–18412. doi: 10.1073/pnas.1305304110

Panchuk, K., Ridgwell, A., and Kump, L. R. (2008). Sedimentary response to Paleocene-Eocene Thermal Maximum carbon release: A model-data comparison. *Geol* 36, 315. doi: 10.1130/G24474A.1

Payne, J. L., Turchyn, A. V., Paytan, A., DePaolo, D. J., Lehrmann, D. J., Yu, M., et al. (2010). Calcium isotope constraints on the end-Permian mass extinction. *Proc. Natl. Acad. Sci.* 107, 8543–8548. doi: 10.1073/pnas.0914065107

Penman, D. E., Turner, S. K., Sexton, P. F., Norris, R. D., Dickson, A. J., Boulila, S., et al. (2016). An abyssal carbonate compensation depth overshoot in the aftermath of the Palaeocene–Eocene Thermal Maximum. *Nat. Geosci* 9, 575–580. doi: 10.1038/ngeo2757

Penn, J. L., Deutsch, C., Payne, J. L., and Sperling, E. A. (2018). Temperature-dependent hypoxia explains biogeography and severity of end-Permian marine mass extinction. *Science* 362, eaat1327. doi: 10.1126/science.aat1327

Percival, L. M. E., Cohen, A. S., Davies, M. K., Dickson, A. J., Hesselbo, S. P., Jenkyns, H. C., et al. (2016). Osmium isotope evidence for two pulses of increased continental weathering linked to Early Jurassic volcanism and climate change. *Geology* 44, 759–762. doi: 10.1130/G37997.1

Percival, L. M. E., Tedeschi, L. R., Creaser, R. A., Bottini, C., Erba, E., Giraud, F., et al. (2021). Determining the style and provenance of magmatic activity during the Early Aptian Oceanic Anoxic Event (OAE 1a). *Global Planetary Change* 200, 103461. doi: 10.1016/j.gloplacha.2021.103461

Pogge Von Strandmann, P. A. E., Jenkyns, H. C., and Woodfine, R. G. (2013). Lithium isotope evidence for enhanced weathering during Oceanic Anoxic Event 2. *Nat. Geosci.* 6, 668–672. doi: 10.1038/ngeo1875

Pogge Von Strandmann, P. A. E., Jones, M. T., Joshua West, A., Murphy, M. J., Stokke, E. W., Tarbuck, G., et al. (2021). Lithium isotope evidence for enhanced weathering and erosion during the Paleocene-Eocene Thermal Maximum. *Sci. Adv.* 7, 4224–4239. doi: 10.1126/sciadv.abh4224

Poulton, S. W., Henkel, S., März, C., Urquhart, H., Flögel, S., Kasten, S., et al. (2015). A continental-weathering control on orbitally driven redox-nutrient cycling during Cretaceous Oceanic Anoxic Event 2. *Geology* 43, 963–966. doi: 10.1130/G36837.1

Remmelzwaal, S. R. C., Dixon, S., Parkinson, I. J., Schmidt, D. N., Monteiro, F. M., Sexton, P., et al. (2019). Investigating ocean deoxygenation during the PETM through the cr isotopic signature of foraminifera. *Paleoceanography Paleoclimatology* 34, 917–929. doi: 10.1029/2018PA003372

Ridgwell, A., Hargreaves, J. C., Edwards, N. R., Annan, J. D., Lenton, T. M., Marsh, R., et al. (2007). Marine geochemical data assimilation in an efficient Earth system model of global biogeochemical cycling. *Biogeosciences* 4, 87–104. doi: 10.5194/bg-4-87-2007

Röhl, U., Westerhold, T., Bralower, T. J., and Zachos, J. C. (2007). On the duration of the Paleocene-Eocene thermal maximum (PETM). *Geochemistry Geophysics Geosystems* 8, Q12002. doi: 10.1029/2007GC001784

Rush, W. D., Kiehl, J. T., Shields, C. A., and Zachos, J. C. (2021). Increased frequency of extreme precipitation events in the North Atlantic during the PETM: Observations and theory. *Palaeogeography Palaeoclimatology Palaeoecol.* 568, 110289. doi: 10.1016/j.palaeo.2021.110289

Sahney, S., and Benton, M. J. (2008). Recovery from the most profound mass extinction of all time. *Proc. R. Soc. B: Biol. Sci.* 275, 759–765. doi: 10.1098/rspb.2007.1370

Shen, S., Cao, C., Zhang, H., Bowring, S. A., Henderson, C. M., Payne, J. L., et al. (2013). High-resolution $\delta^{13}C_{carb}$ chemostratigraphy from latest Guadalupian through earliest Triassic in South China and Iran. *Earth Planetary Sci. Lett.* 375, 156–165. doi: 10.1016/j.epsl.2013.05.020

Shen, S.-Z., Ramezani, J., Chen, J., Cao, C.-Q., Erwin, D. H., Zhang, H., et al. (2019). A sudden end-Permian mass extinction in South China. *GSA Bull.* 131, 205–223. doi: 10.1130/B31909.1

Shen, J., Zhang, Y. G., Yang, H., Xie, S., and Pearson, A. (2022). Early and late phases of the Permian–Triassic mass extinction marked by different atmospheric CO_2 regimes. *Nat. Geosci* 15, 839–844. doi: 10.1038/s41561-022-01034-w

Shields, C. A., Kiehl, J. T., Rush, W., Rothstein, M., and Snyder, M. A. (2021). Atmospheric rivers in high-resolution simulations of the Paleocene Eocene Thermal Maximum (PETM). *Palaeogeography Palaeoclimatology Palaeoecol.* 567, 110293. doi: 10.1016/j.palaeo.2021.110293

Silva-Tamayo, J. C., Lau, K. V., Jost, A. B., Payne, J. L., Wignall, P. B., Newton, R. J., et al. (2018). Global perturbation of the marine calcium cycle during the Permian-Triassic transition. *GSA Bull.* 130, 1323–1338. doi: 10.1130/B31818.1

Slomp, C. P., and Van Cappellen, P. (2007). The global marine phosphorus cycle: sensitivity to oceanic circulation. *Biogeosciences* 4, 155–171. doi: 10.5194/bg-4-155-2007

Song, H., Wignall, P. B., Tong, J., Bond, D. P. G., Song, H., Lai, X., et al. (2012). Geochemical evidence from bio-apatite for multiple oceanic anoxic events during Permian–Triassic transition and the link with end-Permian extinction and recovery. *Earth Planetary Sci. Lett.* 353–354, 12–21. doi: 10.1016/j.epsl.2012.07.005

Song, H., Wignall, P. B., Tong, J., Song, H., Chen, J., Chu, D., et al. (2015). Integrated Sr isotope variations and global environmental changes through the Late Permian to early Late Triassic. *Earth Planetary Sci. Lett.* 424, 140–147. doi: 10.1016/j.epsl.2015.05.035

Stanley, S. M. (2016). Estimates of the magnitudes of major marine mass extinctions in earth history. *Proc. Natl. Acad. Sci.* 113, E6325–E6334. doi: 10.1073/pnas.1613094113

Suan, G., Rulleau, L., Mattioli, E., Suchéras-Marx, B., Rousselle, B., Pittet, B., et al. (2013). Palaeoenvironmental significance of Toarcian black shales and event deposits from southern Beaujolais, France. *Geological Magazine* 150, 728–742. doi: 10.1017/S0016756812000970

Suan, G., van de Schootbrugge, B., Adatte, T., Fiebig, J., and Oschmann, W. (2015). Calibrating the magnitude of the Toarcian carbon cycle perturbation. *Paleoceanography* 30, 495–509. doi: 10.1002/2014PA002758

Sun, H., Xiao, Y., Gao, Y., Zhang, G., Casey, J. F., and Shen, Y. (2018). Rapid enhancement of chemical weathering recorded by extremely light seawater lithium isotopes at the Permian-Triassic boundary. *Proc. Natl. Acad. Sci. United States America* 115, 3782–3787. doi: 10.1073/pnas.1711862115

Tejada, M. L. G., Suzuki, K., Kuroda, J., Coccioni, R., Mahoney, J. J., Ohkouchi, N., et al. (2009). Ontong Java Plateau eruption as a trigger for the early Aptian oceanic anoxic event. *Geology* 37, 855–858. doi: 10.1130/G25763A.1

Them, T. R., Gill, B. C., Caruthers, A. H., Gröcke, D. R., Tulsky, E. T., Martindale, R. C., et al. (2017a). High-resolution carbon isotope records of the Toarcian Oceanic Anoxic Event (Early Jurassic) from North America and implications for the global drivers of the Toarcian carbon cycle. *Earth Planetary Sci. Lett.* 459, 118–126. doi: 10.1016/j.epsl.2016.11.021

Them, T. R., Gill, B. C., Selby, D., Gröcke, D. R., Friedman, R. M., and Owens, J. D. (2017b). Evidence for rapid weathering response to climatic warming during the Toarcian Oceanic Anoxic Event. *Sci. Rep.* 7, 5003. doi: 10.1038/s41598-017-05307-y

Topper, R. P. M., Trabucho Alexandre, J., Tuenter, E., and Meijer, P. T. (2011). A regional ocean circulation model for the mid-Cretaceous North Atlantic Basin: implications for black shale formation. *Climate Past* 7, 277–297. doi: 10.5194/cp-7-277-2011

Trabucho Alexandre, J., Tuenter, E., Henstra, G. A., van der Zwan, K. J., van de Wal, R. S. W., Dijkstra, H. A., et al. (2010). The mid-Cretaceous North Atlantic nutrient trap: Black shales and OAEs. *Paleoceanography* 25, PA4201. doi: 10.1029/2010PA001925

Tsandev, I., and Slomp, C. P. (2009). Modeling phosphorus cycling and carbon burial during Cretaceous Oceanic Anoxic Events. *Earth Planetary Sci. Lett.* 286, 71–79. doi: 10.1016/j.epsl.2009.06.016

Turgeon, S. C., and Creaser, R. A. (2008). Cretaceous oceanic anoxic event 2 triggered by a massive magmatic episode. *Nature* 454, 323–326. doi: 10.1038/nature07076

Ullmann, C. V., Boyle, R., Duarte, L. V., Hesselbo, S. P., Kasemann, S. A., Klein, T., et al. (2020). Warm afterglow from the Toarcian Oceanic Anoxic Event drives the success of deep-adapted brachiopods. *Sci. Rep.* 10, 6549. doi: 10.1038/s41598-020-63487-6

Wallmann, K. (2001). Controls on the cretaceous and cenozoic evolution of seawater composition, atmospheric CO_2 and climate. *Geochimica Cosmochimica Acta* 65, 3005–3025. doi: 10.1016/S0016-7037(01)00638-X

Wang, Y., Cui, Y., Su, H., Jiang, J., Wang, Y., Yang, Z., et al. (2022). Response of calcareous nannoplankton to the Paleocene–Eocene Thermal Maximum in the Paratethys Seaway (Tarim Basin, West China). *Global Planetary Change* 217, 103918. doi: 10.1016/j.gloplacha.2022.103918

Wang, C., Hu, X., Huang, Y., Wagreich, M., Scott, R., and Hay, W. (2011). Cretaceous oceanic red beds as possible consequence of oceanic anoxic events. *Sedimentary Geology* 235, 27–37. doi: 10.1016/j.sedgeo.2010.06.025

Wang, W., Zhang, F., Zhang, S., Cui, Y., Zheng, Q., Zhang, Y., et al. (2023). Ecosystem responses of two Permian biocrises modulated by CO_2 emission rates. *Earth Planetary Sci. Lett.* 602, 117940. doi: 10.1016/j.epsl.2022.117940

Wu, Y., Chu, D., Tong, J., Song, H., Dal Corso, J., Wignall, P. B., et al. (2021). Six-fold increase of atmospheric pCO_2 during the Permian–Triassic mass extinction. *Nat. Commun.* 12, 2137. doi: 10.1038/s41467-021-22298-7

Wu, Y., Cui, Y., Chu, D., Song, H., Tong, J., Dal Corso, J., et al. (2023). Volcanic CO_2 degassing postdates thermogenic carbon emission during the end-Permian mass extinction. *Sci. Adv.* 9, eabq4082. doi: 10.1126/sciadv.abq4082

Zeebe, R. E. (2012). LOSCAR: Long-term Ocean-atmosphere-Sediment CArbon cycle Reservoir Model v2.0.4. *Geosci. Model. Dev.* 5, 149–166. doi: 10.5194/gmd-5-149-2012

Zeebe, R. E., Zachos, J. C., and Dickens, G. R. (2009). Carbon dioxide forcing alone insufficient to explain Palaeocene–Eocene Thermal Maximum warming. *Nat. Geosci* 2, 576–580. doi: 10.1038/ngeo578

Zhang, Y., Mills, B. J. W., He, T., Yang, T., and Zhu, M. (2023). Simulating the long-term carbon cycle in the Phanerozoic: Current status and future developments (in Chinese with English abstract). *Chin. Sci. Bull.* 68, 1580–1592. doi: 10.1360/TB-2022-0813

Zhou, X., Jenkyns, H. C., Owens, J. D., Junium, C. K., Zheng, X.-Y., Sageman, B. B., et al. (2015). Upper ocean oxygenation dynamics from I/Ca ratios during the Cenomanian-Turonian OAE 2. *Paleoceanography* 30, 510–526. doi: 10.1002/2014PA002741